Hindawi
Wireless Communications and Mobile Computing
Volume 2021, Article ID 3635382, 14 pages
https://doi.org/10.1155/2021/3635382

Research Article

An Empirical Study Based on the Impact of Smart Sensor System on Rural Relative Poverty

Tian Luan[1] **and Xiaoyan Liu**[2]

[1]*School of Humanities, Jilin Agricultural University, Changchun, 130118 Jilin, China*
[2]*School of Economics and Trade, JiLin Engineering Normal University, Changchun, 130052 Jilin, China*

Correspondence should be addressed to Xiaoyan Liu; liuxiaoyan@jlenu.edu.cn

Received 25 October 2021; Accepted 4 December 2021; Published 29 December 2021

Academic Editor: Alireza Souri

Solving the problem of rural poverty is a difficult problem for the country to enter a well-off society in an all-round way. Therefore, this paper conducts an experimental analysis based on the impact of smart sensor systems on the relative poverty in rural areas. This article is aimed at studying the related factors of rural poverty and improving relative poverty in rural areas. In this regard, this article proposes an intelligent processing function based on smart sensors. Multiple sensors work together to process relatively complex things. Then, through the experimental analysis of GH efficiency, the data collected in the experimental area is used as the data. Combining the Lorentz curve and Gini coefficient analysis to determine the influencing factors of rural relative poverty. This article also selected 10 areas for experimentation. The experimental results show that the proportion of middle school education from 2014 to 2020 is between 24.3% and 34%, and the number of poor people has also declined, indicating that education level is a factor affecting rural poverty. Therefore, based on the intelligent sensor system, the factors of relative poverty in rural areas can be found, and related measures can be analyzed. By implementing the rural poverty alleviation strategy, the relative poverty situation in rural areas can be effectively improved.

1. Introduction

In recent years, with the rapid development of China's economy and society, rural poverty, especially rural poverty in undeveloped areas in the west and ethnic minority areas, has received extensive attention from relevant state departments and scholars. The existence of poverty has become the primary problem that plagues all countries. Poverty not only hinders economic development but also has a great negative impact on social development. Poverty eradication is a persistent and challenging world problem. Poverty issues have caused uneven development between regions and affected regional peace and stability. How to reduce the incidence of poverty as soon as possible to the greatest extent and improve the life satisfaction and satisfaction of local residents? Happiness is the top issue facing all countries. The relative poverty of peasants, especially those engaged in agriculture, has existed for a long time. Poverty alleviation and development work started from solving the poverty alleviation of the absolute poor, and the relatively poor class was prosperous and prosperous.

In the process of sustained economic development, the income gap between residents is widening and remains at a relatively high level, especially reflecting the severity of relative poverty in rural areas. It can be seen that the income gap between the rich and poor in rural residents' relative movement and deterioration. It has caused a lot of social conflicts and has had a great impact on the development of society. This paper will study rural poverty and antipoverty issues based on the use of smart sensor systems on blockchain theoretical knowledge. On the one hand, it will try to enrich the theoretical research on rural poverty issues in the country. Poverty policy provides theoretical basis.

Wireless Smart Sensor Network (WSSN) shows great promise in structural health monitoring (SHM) due to its low cost, higher flexibility, powerful data management, and

better understanding of structural behavior through dense deployment of sensors. However, the implementation of the wireless SHM system brings many challenges, one of which is to ensure adequate synchronization of the collected data. Li et al. proposed various algorithms to realize the synchronization of clock and sensing [1]. He researched algorithms based on wireless sensors to synchronize clocks and sensing. In order to study the application of smart sensors in fish detection, García et al. designed a smart sensor to predict the established sensory fish quality index. The sensor dynamically correlates the microbial count and TVB-N with the quality index. The sensor provides the largest possible value and handles fish-to-fish variability [2]. His research on fish and microbial detection is very in-depth, but he has little connection with the relative poverty in rural areas. After years of large-scale poverty alleviation and development, the population of extremely poor rural areas across the country has fallen sharply, and the poverty situation has been effectively alleviated. However, due to the large number of poor people, the task of poverty alleviation is still arduous. Therefore, Cao et al. [3] explored the spatial differentiation characteristics and influencing factors of multidimensional poverty in rural areas in a region, which is conducive to the implementation of antipoverty [4] and development strategies and promotes farmers' income and prosperity. Get rid of poverty [5]. Based on the spatial location of the rural areas, the rural poverty factors were searched, but smart sensors were not introduced. Recently, there has been increasing interest in finding durable interventions for rural poverty (RP) in developing countries based on farmers' entrepreneurship and innovation. Therefore, the purpose of Naminse et al. is to test the relationship between entrepreneurship in two resource-constrained provinces in China and the slowdown of RP. He assessed the impact of the three abilities of farm entrepreneurs' education, economy, and social culture on the entrepreneurial growth of farmers and how these abilities in turn affect the mitigation of RP [6]. The impact of intervention on RP can be seen through the evaluation results, but it would be better if smart sensors were added. Safe drinking water is essential to good health. Since long-term drinking can bring health risks, it is important to make recommendations for drinking water sources in areas where CKDu is endemic. Dissanayake et al. designed a sensor to measure fluoride and hardness in well water through an automated mechanism [7]. The sensor he designed is very helpful for detecting water quality. Smart sensor applications rely on ultra-low-power energy harvesters to collect energy and charge batteries within the range of ambient power levels. Wu et al. proposed a discontinuous collection method for switched capacitor DC-DC converters, which can achieve ultra-low-power consumption energy collection. Based on the key observation that energy efficiency is higher than that of charge pumps, he proposed a discontinuous collection technology that can decouple the two efficiencies to obtain a better trade-off [8]. His discontinuous acquisition technology based on smart sensors can improve efficiency very well. All of the above documents are mostly about smart sensor systems. How to combine it to explore the relative poverty factors in rural areas is not very relevant, so this article needs to study in depth based on smart sensor systems to solve rural relative poverty problems.

The innovation of this paper is to use the intelligent processing module function of the intelligent processor to analyze the data of the experimental area for many years. Through the analysis of the data, the factors and influencing factors that affect the poverty in the region can be drawn.

2. Combining Smart Sensors to Study Rural Poverty Factors

2.1. Smart Sensor. Intelligent sensor system [9], the generalized intelligent sensor system is divided into two parts: intelligent sensor terminal and control server [10]. The intelligent sensor terminal uses one or more sensitive components to connect with the embedded microprocessor and completes signal detection and conversion processing through the intelligent sensor terminal, which can realize functions such as self-check, self-calibration, cellular connection, and self-diagnosis. The intelligent sensor terminal [11] and the control server are based on the industrial field bus, using digital communication as the transmission method, with functions such as two-way communication, information processing, and information storage. Most of the functions of the intelligent sensor system are realized by software. By changing the software program of the system and configuring different sensors, different intelligent sensor systems can be realized. A single smart sensor system can also be connected with other smart sensor systems to form a smart sensor system network to jointly complete complex tasks. The intelligent sensor system is shown in Figure 1. Although the smart sensor system will have a low interrupt tolerance problem, this article uses multiple sensors to solve it. When a fault occurs, its working status can be suspended and repaired, but it does not affect the whole. This article mainly applies the consensus technology in the blockchain technology and uses the consensus technology to study and analyze the relative poverty factors in rural areas.

2.1.1. Smart Sensor Vision Measurement. The smart sensor integrates structured optical lasers, cameras, and measurement software [12], which can easily complete scanning, analysis, and measurement functions during the measurement process. Smart sensors use structured light lasers to project structured light on the surface of the object. The distribution of light bars is not straight but varies according to the shape of the object. Collect images and measured values of the structured light bar of the camera at different positions. The schematic diagram of the principle is shown in Figure 2. Next, using image processing technology [13], camera correction technology, structured optical surface correction technology, and laser triangulation measurement principle, the relevant information is extracted from the light strip image, and the three-dimensional coordinates of the object surface are constructed into the light strip, which can be calculated information.

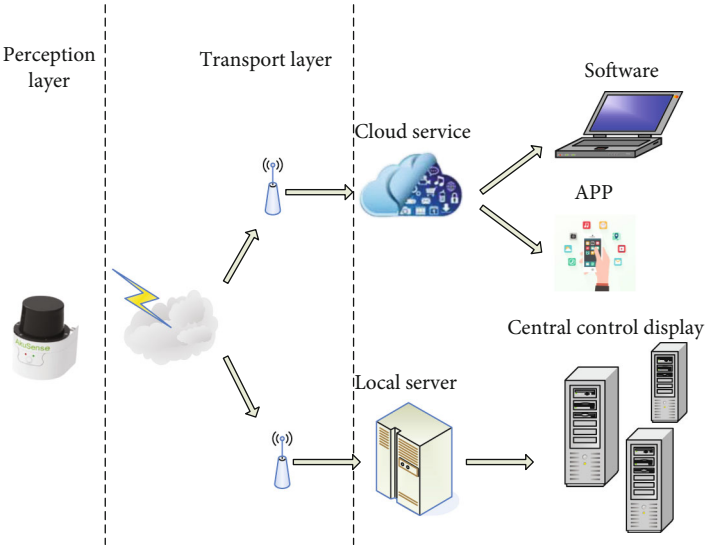

Figure 1: Smart sensor systems.

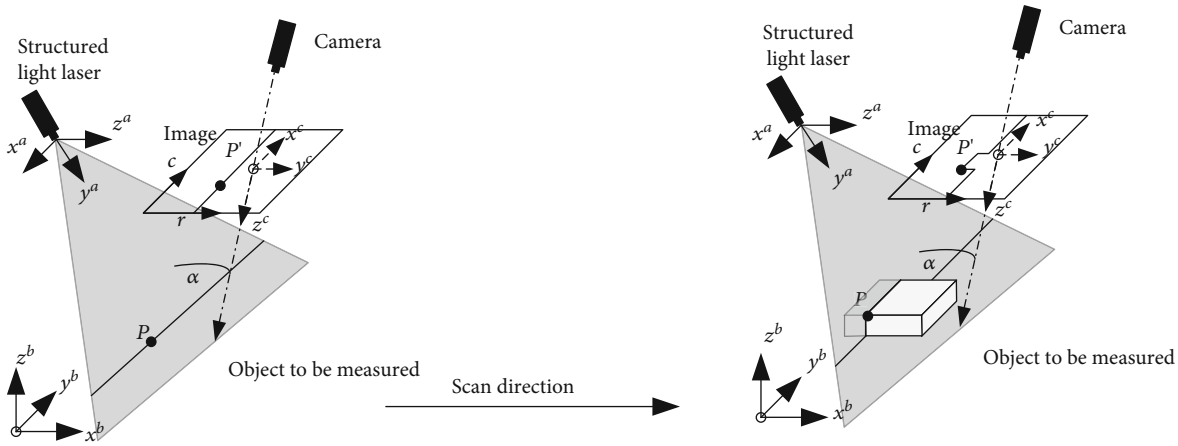

Figure 2: Schematic diagram of smart sensor measurement principle.

(1) Area Scan Camera and Pinhole Camera Model. The perspective projection model of the pinhole camera is shown in Figure 3. The point P of the world coordinate system is projected onto the point P' of the image plane through the optical center of the lens, and the image plane is at a distance f behind the optical center.

(2) Two-Step Calibration Method. The two-stage calibration method proposed by Tsai assumes that the lens has only radial distortion [14]. In the first step of this method, multiple calibration points in the calibration image are used to establish too many decision equations, and a simple matrix theory is used to solve the external parameters of the camera. In the second step, radial distortion parameters are introduced, appropriate initial searchable solutions are set, nonlinear optimization algorithms such as Newton's gradient method are used to solve the nonlinear equation system, and other parameters are solved. In addition, Weng proposed a nonlinear distortion model that takes into account the causes of camera distortion such as radial distortion and eccentric distortion and then uses matrix decomposition methods such as singular value decomposition of the matrix to find the initial values of the camera's internal and external parameters. Search using nonlinear optimization methods. Obtain the most suitable solution for the internal and external parameters of the final camera [15]. In recent years, domestic scholars have also proposed a new two-stage method. Domestic scholars GaoLizhi and ZhanngYanzhen, respectively, proposed a two-stage linear transformation method. Experiments show that the two methods can achieve higher correction accuracy. In the two-stage method of ZYZhang plane calibration board, it is not necessary to extract calibration points on a fixed high-precision calibration platform like the previous two-stage calibration method. His method does not limit the configuration of the calibration board. The posture of the calibration board is arbitrary. At present, this calibration method has been widely used, and both Opencv and Halcon use this method to calibrate cameras.

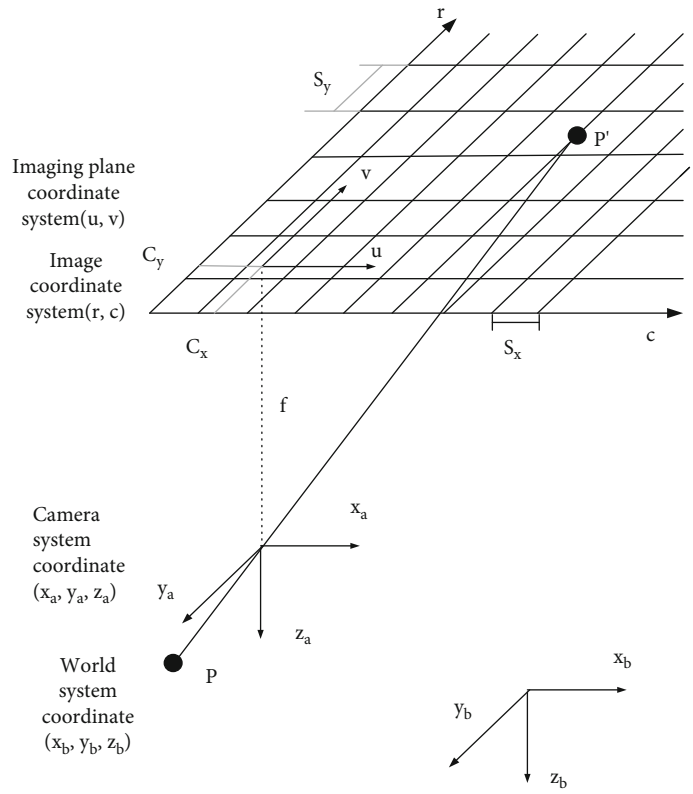

Figure 3: Perspective projection model of pinhole camera

Zhang's calibration method is based on a 2D plane calibration table. This may be a circular grid calibration table or a checkerboard calibration table. Unless the camera selects a lens and changes the focal length and aperture during the calibration process, the internal parameters of the camera will not change, but the external parameters will change. At the same time, the plane on which the calibration sheet is configured must avoid correlation as much as possible. In other words, the calibration table does not move in the plane, but the calibration table needs to be moved in the three-dimensional space plane. During the surface calibration process, the placement position of the calibration sheet is relatively free.

For the disc grid calibration piece, the calibration point is the center of each circle, and for the checkerboard calibration piece, the calibration point is the grid point of the checkerboard grid.

Mark the three-dimensional physical coordinates of the calibration point as $H = [x, y, z]^T$, the corresponding point on the image plane as $h = [u, v]^T$, and the corresponding homogeneous coordinates as $H^{\sim} = [x, y, z, 1]^T$ and $h^{\sim} = [u, v, 1]^T$. Using the pinhole camera model, the three-dimensional space point H can be mapped to the point h in the image coordinate system using equation (1).

$$l\tilde{h} = X[P\,t]\tilde{H}. \tag{1}$$

In the formula, l is any nonzero scale factor, P is the rotation matrix, t is the translation vector, P and t are also the external parameters of the camera, and the internal parameter matrix X is

$$X = \begin{bmatrix} l_x & k & c_x \\ 0 & l_y & c_y \\ 0 & 0 & 1 \end{bmatrix}. \tag{2}$$

Among them, l_x, l_y is the scale factor of the u-axis and the v-axis, p represents the nonperpendicularity of the u-axis and the v-axis, and (c_x, c_y) is the main point. Please note that the thickness of the calibration plate will also affect the calibration accuracy. In order to simplify the description, suppose the thickness of the calibration plate is 0, that is, $z = 0$. The calibration plate is as shown below, on the xy plane of the world coordinate system. Assuming that the i-th column of the rotation matrix P is p_i, from equation (1), we have.

$$l\begin{bmatrix} u \\ v \\ 1 \end{bmatrix} = X[p_1 \quad p_2 \quad p_3 \quad t]\cdot\begin{bmatrix} x \\ y \\ 0 \\ 1 \end{bmatrix} = X[p_1 \quad p_2 \quad t]\cdot\begin{bmatrix} x \\ y \\ 1 \end{bmatrix}. \tag{3}$$

Since $z = 0$, the point H on the plane of the calibration plate can be expressed as $H = [x, y]^T$ and the corresponding homogeneous coordinate $H^{\sim} = [x, y, 1]^T$; then, formula (3)

can be simplified as:

$$l\tilde{h} = M\tilde{H}. \tag{4}$$

In the formula, $M = \lambda X[p_1 \quad p_2 \quad t]$ is a 3×3 matrix, and λ is a constant factor. Remember $M = [m_1 \quad m_2 \quad m_3]$, yes

$$[m_1 \quad m_2 \quad m_3] = \lambda X[p_1 \quad p_2 \quad t]. \tag{5}$$

Among them, t is the translation vector, and the direction of p_1 and p_2 is along the coordinate axis of the image coordinate system. Therefore, p_1 and p_2 are orthogonal, and t and p_1 and p_2 are not coplanar, so $\det([p_1 \quad p_2 \quad t]) \neq 0$. And because of $\det[X] \neq 0$, so $\det[M] \neq 0$.

The calibration point coordinate extracted from the actual image is h_i, and the image coordinate calculated according to the expression (1) is $\tilde{h}_i$. The matrix M can be obtained by solving the minimum distance between the two images.

$$\min \sum_i \left\| h_i - \tilde{h}_i \right\|^2. \tag{6}$$

Use the Levenberg-Marquardt algorithm to solve the above nonlinear quadratic equations to obtain the matrix M, which can be obtained by the orthogonality $(p_1^T p_2 = 0, p_1^T p_1 = p_2^T p_2)$ of equation (5) and P:

$$m_1^T X^{-T} X^{-1} m_2 = 0, \tag{7}$$

$$m_1^T X^{-T} X^{-1} m_1 = m_2^T X^{-T} X^{-1} m_2. \tag{8}$$

Make

$$Y = X^{-T}X^{-1} = \begin{bmatrix} Y_{11} & Y_{12} & Y_{13} \\ Y_{12} & Y_{22} & Y_{23} \\ Y_{13} & Y_{23} & Y_{33} \end{bmatrix} = \begin{bmatrix} \frac{1}{l_x^2} & -\frac{\gamma}{l_x^2 l_y} & \frac{c_y\gamma - c_x l_y}{l_x^2 l_y} \\ -\frac{\gamma}{l_x^2 l_y} & \frac{\gamma^2}{l_x^2 l_y} + \frac{1}{l_x^2} & -\frac{\gamma(c_y\gamma - c_x l_y)}{l_x^2 l_y^2} - \frac{c_y}{l_y^2} \\ \frac{c_y\gamma - c_x l_y}{l_x^2 l_y} & -\frac{\gamma(c_y\gamma - c_x l_y)}{l_x^2 l_y^2} - \frac{c_y}{l_y^2} & \frac{(c_y\gamma - c_x l_y)^2}{l_x^2 l_y^2} + \frac{c_y^2}{l_y^2} + 1 \end{bmatrix}. \tag{9}$$

Please note that Y is a symmetric matrix and can be expressed as the next 6-dimensional vector:

$$y = [\, Y_{11} \quad Y_{12} \quad Y_{22} \quad Y_{13} \quad Y_{23} \quad Y_{33} \,]^T. \tag{10}$$

Suppose the i-th column vector in M is $m_i = [m_{i1}, m_{i2}, m_{i3}]^T$, therefore, there is

$$m_i^T Y m_j = v_{ij}^T y. \tag{11}$$

In

$$v_{ij} = \begin{bmatrix} m_{i1}m_{j1}, m_{i1}m_{j2} + m_{i2}m_{j1}, m_{i2}m_{j2}, m_{i3}m_{j1} \\ + m_{i1}m_{j3}, m_{i3}m_{j2} + m_{i2}m_{j3}, m_{i3}m_{j3} \end{bmatrix}^T. \tag{12}$$

Therefore, the equation system (8) can be rewritten as the following equation system:

$$\begin{bmatrix} v_{12}^T \\ (v_{11} - v_{22})^T \end{bmatrix} \cdot y = 0. \tag{13}$$

If there are n calibration images, the following equations can be formed:

$$Vy = 0. \tag{14}$$

In the above formula, V is a matrix of $2n \times 6$ size. The solution of formula (14) is the intrinsic vector corresponding to the smallest eigenvalue of matrix $V^T V$, and y can also be obtained by performing singular value decomposition (SVD) on matrix V. If y is solved, all the internal parameters of the camera can be obtained according to the following formula:

$$c_y = \frac{(Y_{12}Y_{13} - Y_{11}Y_{23})}{(Y_{11}Y_{22} - Y_{12}^2)}, \tag{15}$$

$$\lambda = \frac{Y_{33} - [Y_{13}^2 + c_y(Y_{12}Y_{13} - Y_{11}Y_{23})]}{Y_{11}}, \tag{16}$$

$$l_x = \sqrt{\frac{\lambda}{Y_{11}}}, \tag{17}$$

$$l_y = \sqrt{\frac{\lambda Y_{11}}{(Y_{11}Y_{22} - Y_{12}^2)}}, \tag{18}$$

$$\gamma = \frac{-Y_{12}l_x^2 l_y}{\lambda}, \tag{19}$$

$$c_x = \frac{\gamma c_y}{l_x} - \frac{Y_{13}l_{x^2}^2}{\lambda}. \tag{20}$$

(3) Multisensor Information Fusion Structure. Multisensor information fusion [16] can process multiple levels of information through a variety of methods, so it is necessary to investigate the corresponding hardware topology. Multisensor information fusion can be divided into centralized fusion system, decentralized fusion system, hybrid fusion system, and feedback fusion system. This article uses a multisensor structure for information fusion and uses multiple sensors to collaborate to complete data collection.

(1) Centralized

The centralized information fusion system [17] directly performs fusion inference on the observation data of multiple sensors without any preprocessing, and its structure is shown

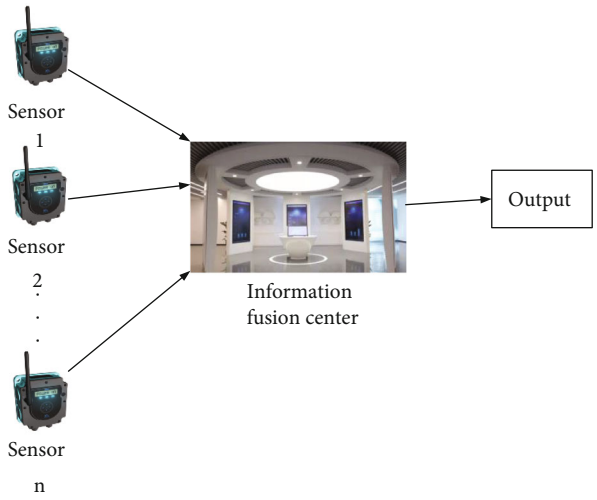

Figure 4: Centralized fusion system structure diagram.

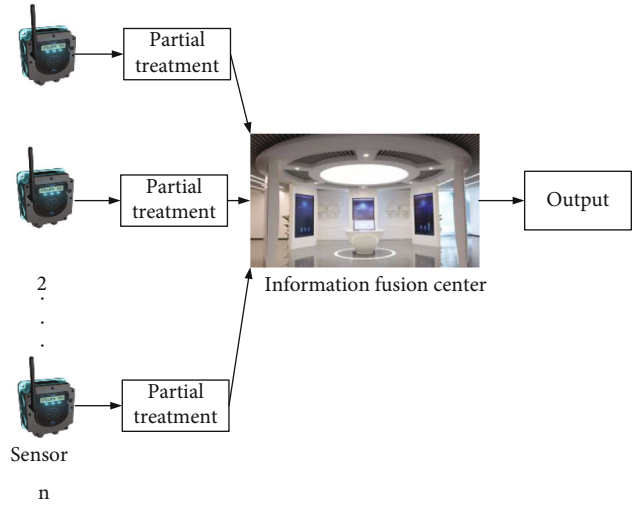

Figure 5: Structure diagram of distributed fusion system.

in Figure 4. Centralized information fusion belongs to the data layer fusion, which retains a large amount of original data, so the fusion accuracy is very high, but the fusion center needs to identify and reason a large amount of data, and the communication volume is large, and the processor design is complex, so this structure is suitable for small-scale integration systems.

(2) Distributed

Distributed information fusion system [18] refers to the calculation, classification, or inference processing of each sensor data separately and then transfers the processed data results to the fusion center, and the fusion center completes the final reasoning judgment. This method is similar to feature layer fusion or decision layer fusion. Due to the large amount of distributed preprocessing of sensor data, the fusion center has fewer tasks and at the same time reduces the amount of data transmission. This method is suitable for large-scale distributed remote fusion systems. Its structure is shown in Figure 5.

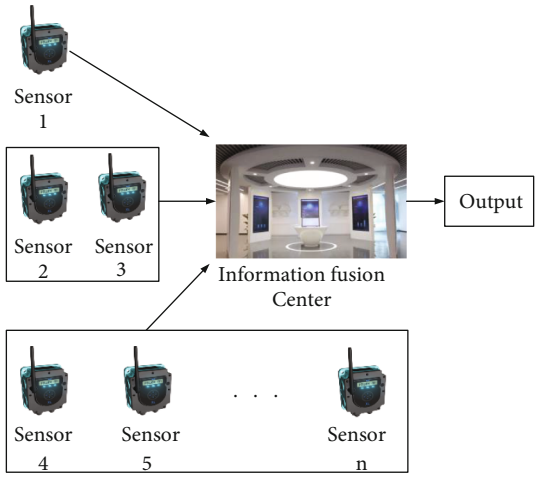

Figure 6: Structure diagram of hybrid fusion system.

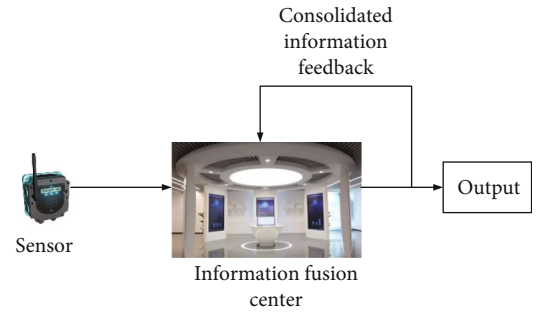

Figure 7: Feedback type multisensor information fusion structure.

(3) Hybrid

The hybrid information fusion system [19] is a mixed use of distributed and centralized types. It uses a centralized structure for some sensors and a distributed structure for some sensors. It has the advantages of distributed and centralized fusion structures, and the system structure is flexible. A more accurate fusion result can be obtained, but the structure of the system is complex, and the design is difficult. How to choose depends on the specific situation. Its structure is shown in Figure 6.

(4) Feedback type

The feedback information fusion system [20] feeds back the fusion result to the fusion system to form a closed-loop system with certain self-regulating ability. With this structure, after the fusion center processes the sensor information, the fusion system can already express most of the characteristics of the target object, so it has a better guiding effect on the newly acquired information. Its structure is shown in Figure 7.

2.2. GH Efficiency. For GH efficiency, in the Normal-OperationCase phase of PBFT, a total of $PM = 2x^2$ messages are needed to complete the final consensus, and the message complexity is $o(n^2)$. GH splits Normal-OperationCase into three steps.

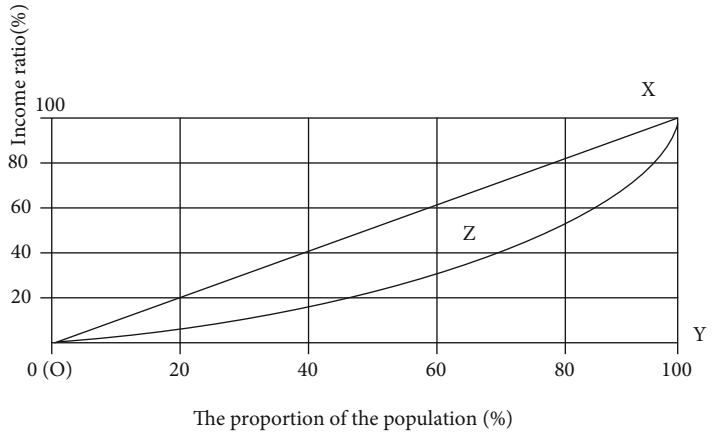

Figure 8: Lorentz curve.

(1) Globally accept the request message, yp arranges the global serial number, locally executes localprepare and localcommit, and GH changes the original process of pairwise interaction across the entire network to pairwise interaction within the group, reducing the number of messages that each node needs to send and waiting for messages The total number of messages consumed in this step:

$$2\sum_{j=1}^{j=y} m_j^2 - x + y - 1. \tag{21}$$

(2) Cross-submission between copies, namely, intersectional reply, consumes the number of messages:

$$y(x-1). \tag{22}$$

(3) The global replica node executes globalprepare, globalcommit, globalreply, and the number of messages consumed:

$$2y^2 - 2y + 1. \tag{23}$$

Until the request is finally completed, the number of messages GM consumed in the GH consensus phase is synthesized from formulas (21), (22), and (23):

$$\mathrm{GM} = 2\sum_{j=1}^{j=y} m_j^2 - x + y - 1, \tag{24}$$

$$\mathrm{GM} = 2\frac{x^2}{y} + 2z^2 + 2y^2 + y(x-2)x, \tag{25}$$

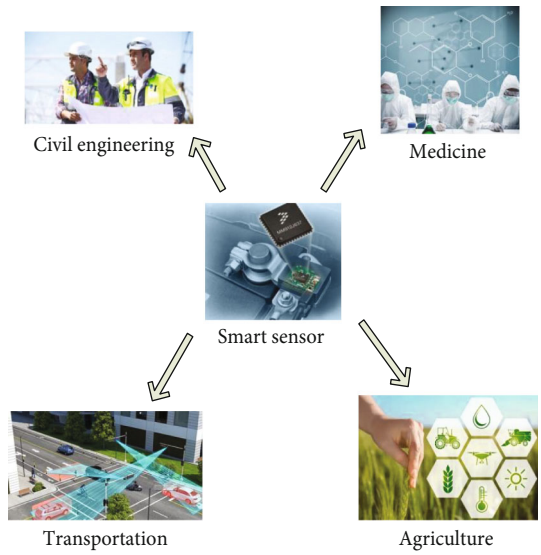

Figure 9: Application areas of smart sensors.

where z is the variance and the formula () knows that z is 0, which means that the number of messages consumed in the GH consensus phase is the least when the group is averaged:

$$\mathrm{GM} = 2\frac{x^2}{y} + 2y^2 + y(x-2)x, \tag{26}$$

$$\frac{\partial \mathrm{GM}}{\partial y} = -2\frac{x^2}{y^2} + 4y + x - 2 = 0. \tag{27}$$

2.3. Measurement of Poverty Level. To study the poverty of a region, we should first fully grasp the poverty level of the region, that is, how poor the region is. Here is a brief introduction to several methods of measuring poverty.

2.3.1. Incidence Rate of Poverty. Also known as the head calculation index, it calculates the proportion of people whose income is below the absolute poverty line in the total population based on urban and rural income distribution data. The formula can be expressed as $\mathrm{PH} = p/n$,

Table 1: Number of poor populations in 10 regions.

Area	1	2	3	4	5	6	7	8	9	10
Population	29.41	13.14	11.16	2.63	7.89	15.33	14.86	14.91	18.71	7.24
Change from last year	-0.63	-1.53	-0.65	-0.26	-0.63	-1.03	0.08	-1.78	-2.22	-0.54

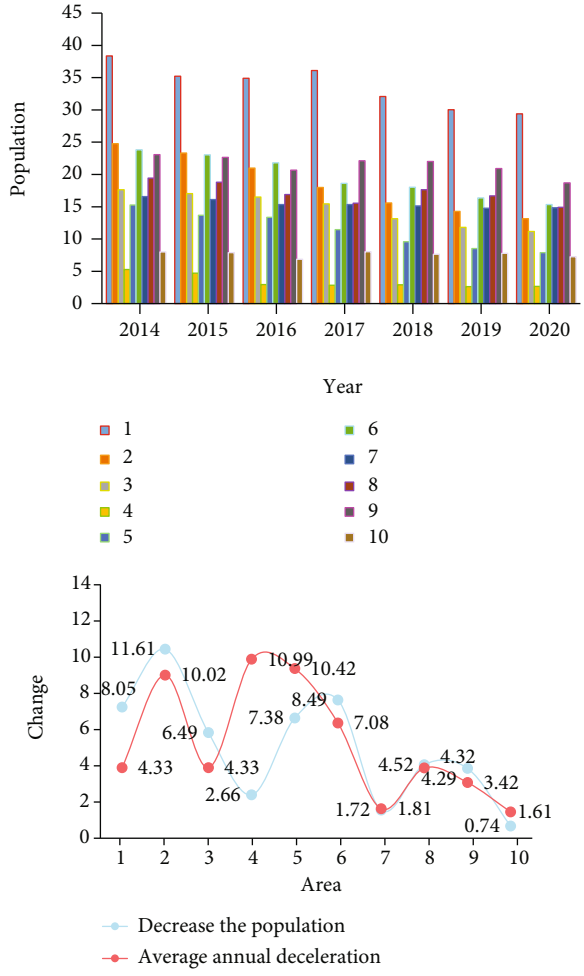

Figure 10: Population changes in ten regions in the past 7 years.

where n is the total population and p is the number of people below the absolute poverty line. The poverty incidence rate is used to determine the size and change of the poor population on the cross-section of the poverty line. The basic feature is that the income changes and income distribution of the population below the poverty line are not considered. The focus is on determining the proportion of the population. Therefore, the disadvantage of this indicator is that it cannot reflect the income reduction and income transfer of the poor.

2.3.2. Poverty Gap Rate. In order to make up for the insufficiency of the poverty incidence rate in determining the poverty level, the poverty gap rate is used to measure the degree to which the poor's income is below the poverty line. Therefore, this indicator is also called the poverty gap ratio or relative poverty index, and its formula is expressed as:

$$\mathrm{PG} = \sum_{k}^{n} \frac{((1 - Yk)/Z)}{n}. \tag{28}$$

Among them, Yk represents the consumption level or income of the k-th poor, Z represents the poverty line, and n represents the total population. It can be deduced from the formula that this method can sensitively measure the degree of poor people below the poverty line and make up for the lack of poverty incidence, but it cannot reflect the population size, proportion, and distribution of poverty status.

2.3.3. Poverty Intensity Index. The poverty intensity index is also known as the FGT index. It is based on the distance of the poor relative to the poverty line. It just gives the poor a greater weight to calculate their poverty level. The calculation formula is

$$\mathrm{FGT} = \sum_{k=1}^{n} \frac{((1 - Yk)/Z)^2}{n}. \tag{29}$$

2.3.4. Sen Index. In order to avoid the shortcomings of the above two indicators [21], the well-known Indian economist Sen seeks a measurement method that integrates the headcount index, the poverty gap, and the degree of inequality in the poor population, which is called the Sen index [22]. The formula is

$$P = \frac{k}{\mathrm{KZ}}[Z - x(1 - G)], \tag{30}$$

or

$$P = \mathrm{PH}\left[\frac{1 - x(1 - G)}{Z}\right]. \tag{31}$$

Among them, k is the number of the poor, K is the total population, Z is the poverty line, x is the average income of the poor, and G is the Gini coefficient of the income distribution of the poor. The value of P changes from 0 to 1. If everyone's income exceeds the poverty line, $n = 0$, and $P = 0$; if everyone has no income or the social distribution is extremely unequal, $x = 0$, $k = 0$, $G = 1$, and $P = 1$.

2.3.5. Lorentz Curve and Gini Coefficient. This is a method often used to evaluate relative poverty, and it reflects the degree of inequality in income distribution.

(1) Lorentz Curve. The Lorenz curve is a curve composed of population proportions and corresponding income proportions, used to express equality of income and distribution. It was first proposed by the American statistician M.O.

Table 2: Changes in income and population in experimental areas.

Years	Poor people			Low income		
	Total people	The rate of decline	Reduce the number of people	Total people	The rate of decline	Reduce the number of people
2014	196.03			560.40		
2015	188.82	-3.68	7.21	523.46	-6.59	36.94
2016	176.89	-6.32	11.93	471.16	-9.99	52.3
2017	169.32	-4.28	7.57	442.42	-6.10	28.74
2018	158.86	-6.18	10.46	397.95	-10.05	44.47
2019	148.54	-6.50	10.32	355.32	-10.71	42.63
2020	139.41	-6.15	9.13	316.57	-10.91	38.75
Average value		-6.59	9.44		-10.79	40.64

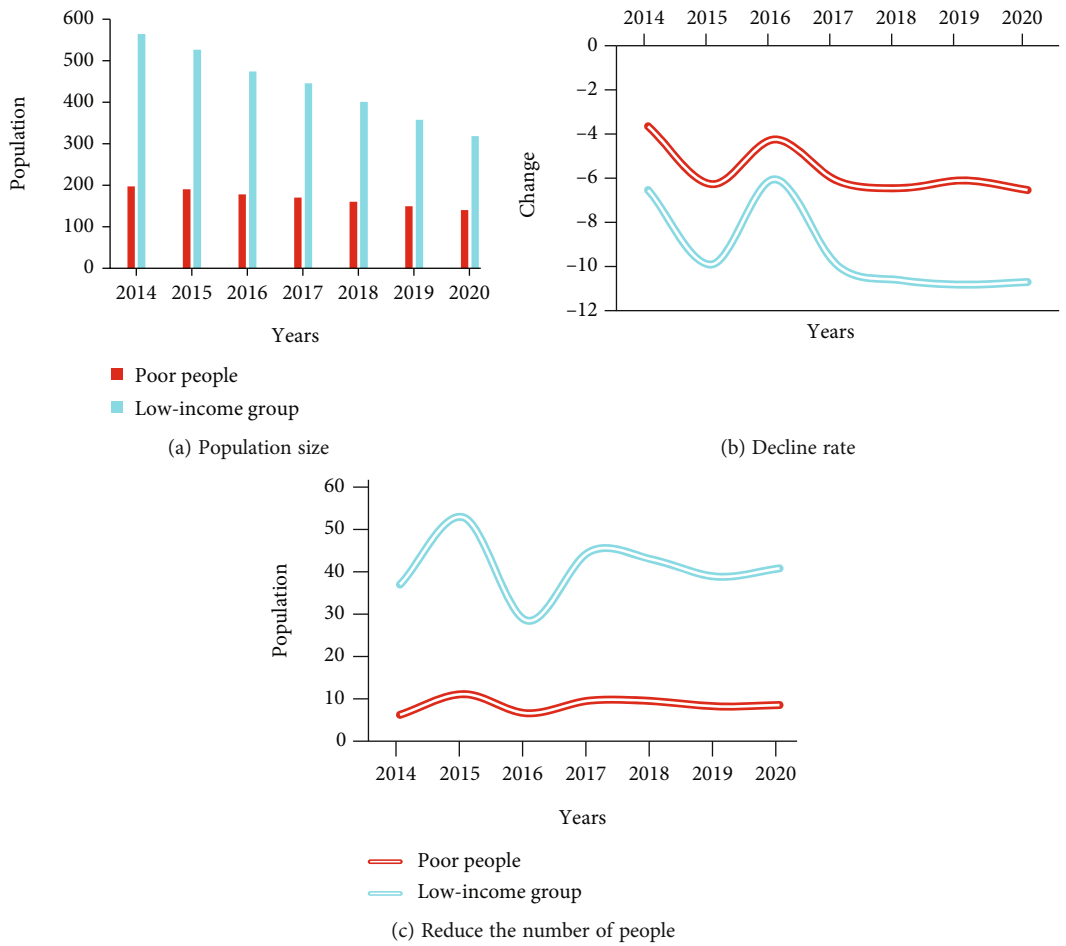

Figure 11: Changes in the poor population and low-income population in the experimental area.

Table 3: Sex change ratio of rural population in experimental areas (unit: %).

Years	Male ratio	Proportion of women	Sex ratio
2014	51.6	48.4	106.7
2020	50.9	49.2	103.2

Lorentz in 1907, so it was named the Lorentz curve. The Lorentz curve can be represented in Figure 8.

In the above rectangular coordinate system, the horizontal axis represents the proportion of the population sorted by income from low to high, and the level axis represents the proportion of income occupied by the corresponding proportion of the population. The straight line OX in the figure

Table 4: Changes in education level (unit: %).

Education level	2014	2020
Illiteracy	23.8	13.8
Primary school	46.0	43.2
Junior high school	24.3	34.0
High school	5.5	7.4
College	0.4	1.3
Undergraduate	0.04	0.37
Postgraduate	0.006	0.01

is called a complete equality line, because the vertical and horizontal coordinates of each point on OX are equal, which means that a certain proportion of the population has an equal proportion of income. For example, 20% of the population has 20% of the income. In other words, in this state, incomes are completely equal. The broken line 0-Y-X is the absolute inequality line, because the income of all proportions of the population is 0, and the income is completely occupied by one person. Therefore, when the Lorentz curve coincides with OX, it means that the income in the region is completely equal; when it coincides with 0-Y-X, it represents absolute income inequality. The general Lorentz curve is between these two lines, indicating that income is not completely equal. Reflected in the figure is a curve, and the degree of curvature of the curve indicates the level of income inequality. According to experiments, the closer to the OX line, the more equal the income; the closer to the 0-Y-X line, the more unequal the income.

(2) Gini Coefficient. The Gini coefficient is the first measurement of income distribution equality defined by Italian economists based on the Lorenz curve, and it is now the most commonly used indicator to measure income inequality. In the above Figure 9 Lorentz curve, the area enclosed by the complete equation line OX and the Lorentz curve is called the inequality area; X is marked as X; if the area below the OX ray is marked as Y, it is the Gini coefficient $G. = X/Y$. The Gini coefficient is between 0 and 1. Experiments show that the smaller the value, the smaller the income gap, the higher the degree of income equality, and vice versa. Generally speaking, $G < 0.2$, the income distribution is very even, $0.2 \le G < 0.3$, the income distribution is relatively equal, $0.3 \le G < 0.4$, the income distribution is relatively equal, $0.4 \le G < 0.5$ has a large income gap, $G > 0.5$, and the income gap is large; the inequality of income distribution is relatively large. Among them, it is generally considered that $G = 0.4$ is the warning line, and society will become unstable if it exceeds 0.4.

In addition, the commonly used Gini coefficient calculation formula is

$$G = \frac{1}{2\mu k^2}\sum_{i=1}^{k}\sum_{j=1}^{k}|yi - yj|, \tag{32}$$

where k is the sample size, μ is the expected value of the total income of each sample group, and $|yi - yj|$ represents the absolute value of the income difference between any two samples.

3. Experiments to Explore the Relative Influencing Factors of Poverty Based on Smart Sensors

Intelligent sensor system, this is a comprehensive high-tech that is rapidly developing in the world today. The central idea is to use computer technology to make sensors intelligent. It is generally believed that the intelligent sensor system is detection, measurement, and control system composed of sensors, computer technology, and communication technology. Its main application is shown in Figure 9.

3.1. Number of Poor People. In this paper, 10 regions are selected as samples for the experiment, and the methods of investigating poverty influencing factors with smart sensors are carried out in 10 regions, respectively. The number of poor people in these 10 regions is shown in Table 1 (unit: ten thousand people). In order to better analyze the poverty indicators of these regions in the past, the changes in the region from 2014 to 2020 are as follows, as shown in Figure 10.

It can be seen from the figure that the total number of poor people in the 10 regions is declining. In particular, the rate of poverty reduction in regions 1 and 2 is very fast, and the rate of poverty reduction in regions 7, 8, 9, and 10 is quite slow. Choose one of them to analyze the impact of poverty factors through the method of this article.

3.2. Experiments to Explore Changes in the Poor Population. The selected region's low-income population changes are shown in Table 2 (unit: ten thousand people, %).

Through the collected data, we can get Figure 11, as shown in the figure.

It can be seen from the above table that although the overall poverty population has shown a downward trend, with a decrease of 70,000 to 100,000 poor populations every year, the rate of poverty reduction is relatively slow, generally maintained at around 6%, which is in line with the national average annual deceleration of 11.79%. Among them, there was a slowdown in 2017 and 2020.

3.3. Gender Structure and Education Level of the Experimental Area. Different genders have different social functions, so the characteristics of gender structure are also one of the important reasons that affect the future development of rural areas. The proportion of men and women in the rural population in the experimental areas was basically the same. From 2000 to 2006, the proportion of men in the population declined slightly, from 51.6% in 2000 to 50.9%, and the proportion of women in the population rose slightly, from 48.4% in 2000 to 50.9%. As shown in Table 3.

Education has always been the main way to invest in human capital. The level of rural education largely reflects the level of human capital. According to the 2014 and 2020

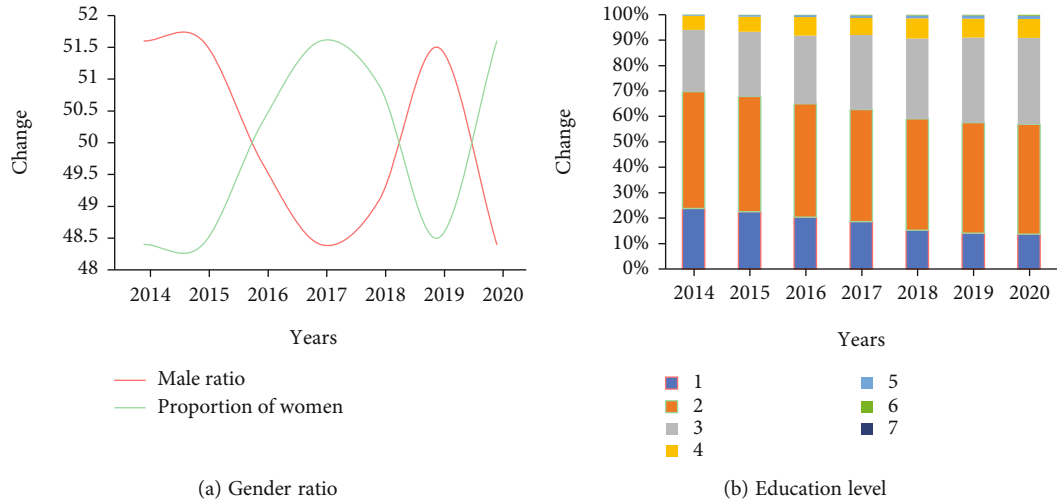

(a) Gender ratio (b) Education level

Figure 12: Rural gender ratio and educational level year-by-year ratio.

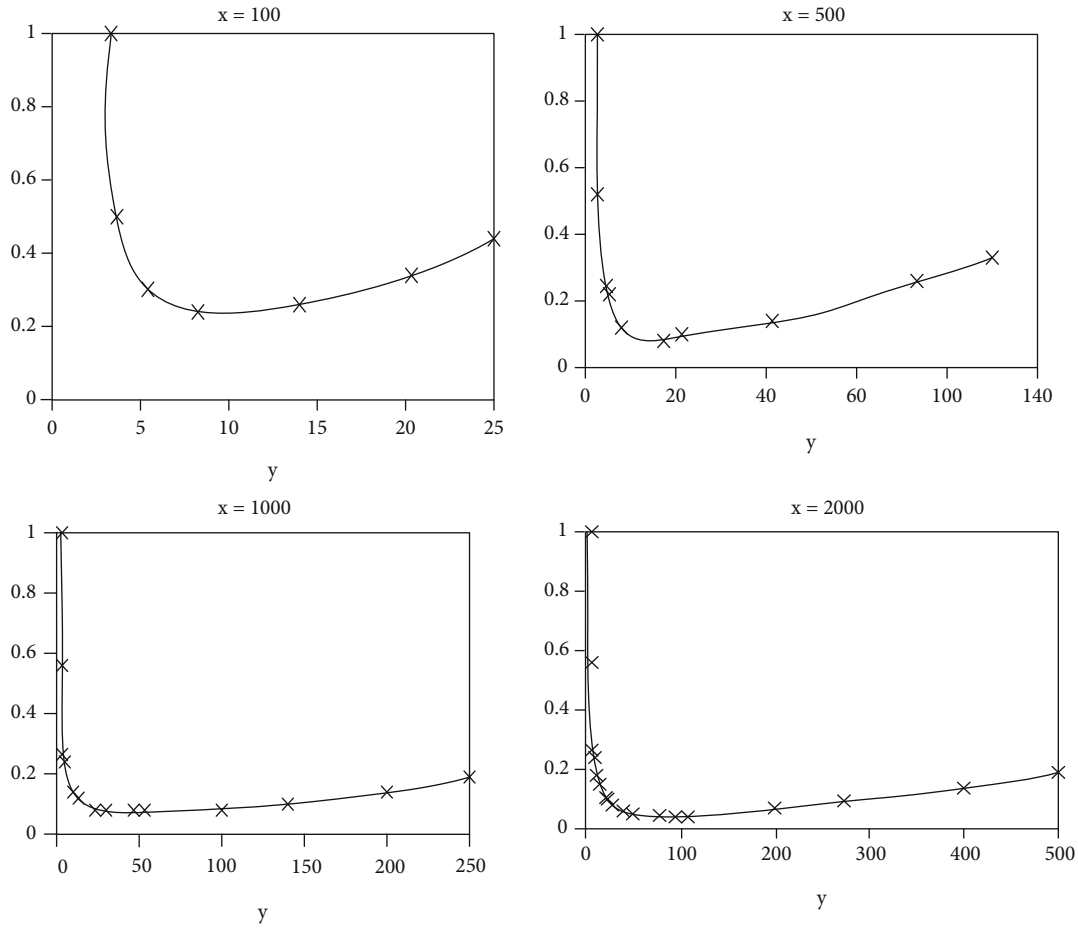

Figure 13: GM/PM.

census data, the overall educational level of the rural population over 6 years old in the experimental areas has increased. The proportion of illiterate and elementary school population has decreased year by year. The proportion of Chinese illiterate population has dropped from 23.8% in 2014 to 13.8% in 2020, which is a significant decline. The proportion of population in elementary school has also dropped from 46.0% in 2014 to 43.2%. The proportion of the population

Table 5: Poverty factors in experimental areas.

Factor	Poor households	Percentage (%)	Number of poor	Percentage (%)
Disease	687	44.39	1285	39.96
Disability	82	5.22	160	4.97
Lack of labor	188	11.97	269	8.36
Study	5	0.31	17	0.52
Technology, capital	442	28.15	1077	33.49
Traffic condition	24	0.89	23	0.71
Insufficient motivation for own development	24	1.52	77	2.39
Lack of land	97	6.17	260	8.08
Other reasons	11	0.70	47	1.46

with junior high school, high school, and above education level is on the rise. Among them, the proportion of the junior high school population has increased significantly, from 24.3% in 2014 to 34.0% in 2020. From the data, it can be seen that the rural population in Gansu Province is dominated by elementary and junior high school education, as shown in Table 4.

Through experiments, we analyzed the impact of gender and education level on rural poverty, as shown in Figure 12 (1 is illiteracy, 2 is primary school, 3 is junior high school, 4 is high school, 5 is college, 6 is undergraduate, and 7 is postgraduate).

It can be seen from the figure that the gender ratio has little effect on rural poverty, but the level of education is very much related to the impact of poverty. As the average per capita education gradually increases, the rural poor population is also decreasing. By the beginning of 2020, the educational background has reached 34%, which is 9.7% higher than the 24.3% in 2014. This shows that the higher the education level of rural people, the higher the income.

4. Data Collection Experiment Results

4.1. GH Efficiency and Safety Analysis. From the GH efficiency, it can be concluded that y and x satisfy the formula () as the best grouping. According to the $3f + 1$ model, it is concluded that the total number of copies of the system $x > 4$. Taking $x = 100$, $x = 500$, $x = 1000$, and $x = 2000$ as an example, the consumption message comparison between GH and PBFT is shown in Figure 13.

For GH packet security, the purpose of the GH packet protocol is to divide distributed nodes into multiple partitions, and each partition executes the GH consensus protocol in parallel to improve consensus efficiency. The analysis of the group security is as follows:

(1) Fast grouping is not a combination of yp completely arranging replica nodes of the entire network, which prevents the worst grouping state from being, arranged when the master node is a Byzantine node. At the same time, each replica node is not allowed to be freely combined, which can further improve the grouping speed and also allow other lps to choose their own lx according to the specific situation

(2) The condition for successful group establishment is at least 2mj/3 consistent messages to ensure that each group satisfies the $3f + 1$ model. Since each group is built in a closed form, Gj returns a BACKWARD message to Gj-1. All subsequent groups were successfully formed. In order to prevent a group from being sandwiched between the two normal groups, whose lp is a Byzantine node or the link is broken due to other benign errors, the Backward phase is designed. If the BackwardTimer expires, the message <BREAKPOINT-FINDING is sent, $T > \sigma i$ to ensure that the grouping status of replica nodes in the entire network remains uniform even if there is a broken link

(3) According to the $3f + 1$ model, in PBFT, if the number of normal nodes, benign and wrong non-Byzantine nodes, and Byzantine nodes each account for 1/3, the remaining last node can control the consensus result of the entire network. GH reduces the influence of the last node and Byzantine node after the entire network is grouped to the group it is in instead of the entire network

(4) GH adopts self-closing mechanism to stabilize the total number of Byzantine nodes in the system below the critical point 1, and the number of Byzantine nodes in the group stabilizes at mj/3 + 1. At the same time, a suspicion zone is set. When the system performs safe grouping between critical point 1 and critical point 2, it makes full use of the fault tolerance of each group

4.2. Poverty Factors. After analyzing the efficiency of smart sensors under the blockchain theory, the data in the experimental area is analyzed, and Table 5 can be shown.

From the data in the table, it can be concluded that 44.39% of people are poverty-stricken due to diseases, and 33.49% are due to technology and funds. Therefore, the most important way to get rid of poverty is to develop technological development. Only by possessing feasible technology can rural areas be transformed into poverty. Chengcheng will allow rural people to lead a prosperous life and no longer suffer from poverty.

5. Conclusions

Rural poverty is a problem that the country is studying, but this problem has not yet been resolved. Based on smart sensors, this paper collects and analyzes data and analyzes and experiments on the factors that affect rural poverty through the intelligent processing of smart sensors. The experimental results show that the educational level of the rural population is closely related to their income. The experimental results show that the higher the level of education, the higher the income, and the smaller the number of poor people. This experiment selects a region for data analysis. Through analysis, its junior high school education rate has increased from 24.3% in 2014 to 34% in 2020, and the poverty population has also decreased. Moreover, through the intelligent processing of smart sensors, it can be concluded that 44.39% of the rural population is impoverished due to diseases, and 33.49% is impoverished due to technology and funds. Therefore, as long as the right medicine is prescribed, the rural people can get rid of the poverty of the rural people. Get rid of poverty, keep pace with the times, and fight the tough battle against poverty with the country.

Data Availability

No data were used to support this study.

Conflicts of Interest

The authors state that this article has no conflict of interest.

Acknowledgments

This work was supported by the Doctoral Research Initiation Funding Project of Jilin Engineering Normal University (Project number: BSSK202001), the Rural Development Institute of JiLin Engineering Normal University, and the Program for Innovative Research Team of JiLin Engineering Normal University.

References

[1] J. Li, K. A. Mechitov, R. E. Kim, and B. F. Spencer Jr., "Efficient time synchronization for structural health monitoring using wireless smart sensor networks," *Structural Control and Health Monitoring*, vol. 23, no. 3, pp. 470–486, 2016.

[2] M. R. García, M. L. Cabo, J. R. Herrera, G. Ramilo-Fernández, A. A. Alonso, and E. Balsa-Canto, "Smart sensor to predict retail fresh fish quality under ice storage," *Journal of Food Engineering*, vol. 197, no. mar., pp. 87–97, 2017.

[3] B. Cao, X. Wang, W. Zhang, H. Song, and Z. Lv, "A many-objective optimization model of industrial Internet of Things based on private blockchain," *IEEE Network*, vol. 34, no. 5, pp. 78–83, 2020.

[4] W. D. du, S. L. Pan, D. E. Leidner, and W. Ying, "Affordances, experimentation and actualization of FinTech: a blockchain implementation study," *The Journal of Strategic Information Systems*, vol. 28, no. 1, pp. 50–65, 2019.

[5] J. Cai, Y. Yu, D. Luo et al., "Space differentiation and its influence factor analysis of rural multidimensional poverty in Chongqing," *Nongye Gongcheng Xuebao/Transactions of the Chinese Society of Agricultural Engineering*, vol. 34, no. 22, pp. 235–245, 2018.

[6] E. Y. Naminse, J. Zhuang, and F. Zhu, "The relation between entrepreneurship and rural poverty alleviation in China," *Management Decision*, vol. 57, no. 9, pp. 2593–2611, 2019.

[7] S. Dissanayake, H. Pasqual, and B. Athapattu, "Economical colorimetric smart sensor to measure water quality of drinking water in CKDu prevalence areas," *IEEE Sensors Journal*, vol. 17, no. 18, pp. 5885–5891, 2017.

[8] X. Wu, Y. Shi, S. Jeloka et al., "A 20-pW discontinuous switched-capacitor energy harvester for smart sensor applications," *IEEE Journal of Solid-State Circuits*, vol. 52, no. 4, pp. 972–984, 2017.

[9] B. Markey-Towler, "Anarchy, Blockchain and Utopia: a theory of political-socioeconomic systems organised using Blockchain," *The Journal of British Blockchain Association*, vol. 1, no. 1, pp. 1–14, 2018.

[10] A. Paliwal, A. Laborte, and N. M. Paguirigan, "Rural poverty and rice," *Rice Today*, vol. 15, Supplement 1, pp. 30-31, 2016.

[11] Y. Wang, M. Singgih, J. Wang, and M. Rit, "Making sense of blockchain technology: how will it transform supply chains?," *International Journal of Production Economics*, vol. 211, no. - MAY, pp. 221–236, 2019.

[12] A. I. Torre-Bastida, J. Díaz-de-Arcaya, E. Osaba, K. Muhammad, D. Camacho, and J. del Ser, "Bio-inspired computation for big data fusion, storage, processing, learning and visualization: state of the art and future directions," *Neural Computing and Applications*, 2021.

[13] R. Santos, "On the philosophy of bitcoin/blockchain technology: is it a chaotic, complex system?," *Social Science Electronic Publishing*, vol. 48, no. 5, pp. 620–633, 2017.

[14] M. Swan and P. de Filippi, "Toward a philosophy of blockchain: a symposium: introduction," *Metaphilosophy*, vol. 48, no. 5, pp. 603–619, 2017.

[15] K. Lo, L. Xue, and M. Wang, "Spatial restructuring through poverty alleviation resettlement in rural China," *Journal of Rural Studies*, vol. 47, Part B, pp. 496–505, 2016.

[16] A. G. Naimanye and T. Whiteing, "Poverty-centred rural road funds sharing in sub-Saharan Africa," *Proceedings of the Institution of Civil Engineers*, vol. 169, no. 6, pp. 387–396, 2016.

[17] P. O.-W. Adjei, D. Buor, and P. Addrah, "Ecological health effects of rural livelihood and poverty reduction strategies in the Lake Bosomtwe basin of Ghana," *Geo Journal*, vol. 82, no. 3, pp. 609–625, 2017.

[18] S. Sharaunga, "The effectiveness of women's skills development to household poverty reduction: the case of Msinga rural areas," *Poverty & Public Policy*, vol. 11, no. 1-2, pp. 73–98, 2019.

[19] B. Hou, H. Liao, and J. Huang, "Household cooking fuel choice and economic poverty: evidence from a nationwide survey in China," *Energy and Buildings*, vol. 166, pp. 319–329, 2018.

[20] T. Potocki and M. Cierpial-Wolan, "Factors shaping the financial capability of low-income consumers from rural regions of Poland," *International Journal of Consumer Studies*, vol. 43, no. 2, pp. 187–198, 2019.

[21] S. Naha, S. P. Wu, and S. Velmathi, "Naphthalimide based smart sensor for CN−/Fe3+and H2S. Synthesis and

application in RAW264.7 cells and zebrafish imaging," *Advances*, vol. 10, no. 15, pp. 8751–8759, 2020.

[22] S. Famila, A. Jawahar, A. Sariga, and K. Shankar, "Improved artificial bee colony optimization based clustering algorithm for SMART sensor environments," *Peer-to-Peer Networking and Applications*, vol. 13, no. 4, pp. 1071–1079, 2020.